Microstructure Refinement After the Addition of Titanium Particles in AZ31 Magnesium Alloy Resistance Spot Welds

L. XIAO, L. LIU, S. ESMAEILI, and Y. ZHOU

Microstructural evolution of AZ31 magnesium alloy welds without and with the addition of titanium powders during resistance spot welding was studied using optical microscopy, scanning electron microscopy, and transmission electron microscopy (TEM). The fusion zone of AZ31 magnesium alloy welds could be divided into columnar dendritic zone (CDZ) and equiaxed dendritic zone (EDZ). The well-developed CDZ in the vicinity of the fusion boundary was clearly restricted and the coarse EDZ in the central region was efficiently refined by adding titanium powders into the molten pool, compared with the as-received alloy welds. A microstructural analysis showed that these titanium particles of approximately 8 μm diameter acted as inoculants and promoted the nucleation of α-Mg grains and the formation of equiaxed dendritic grains during resistance spot welding. Tensile-shear testing was applied to evaluate the effect of titanium addition on the mechanical properties of welds. It was found that both strength and ductility of magnesium alloy welds were increased after the titanium addition. A TEM examination showed the existence of an orientation matching relationship between the added Ti particles and Mg matrix, *i.e.*, $[01\bar{1}0]_{Mg}//[1\bar{2}1\bar{3}]_{Ti}$ and $(0002)_{Mg}//(10\bar{1}0)_{Ti}$ in some grains of Ti polycrystal particles. This local crystallographic matching could promote heterogeneous nucleation of the Mg matrix during welding. The diameter of the added Ti inoculant should be larger than 1.8 μm to make it a potent inoculant.

DOI: 10.1007/s11661-011-0881-y

I. INTRODUCTION

AS the lightest of available structural metallic materials, magnesium (Mg) alloys are being considered for structural components of automobiles becasue of the strong demand for reducing vehicle weight for better fuel efficiency. However, resistance spot welding (RSW), which is a widely used joining technique in the automotive industry, frequently results in the formation of well-developed columnar grains in the vicinity of fusion boundaries and coarse equiaxed dendritic grains in the central region of AZ31 Mg alloy welds.[1–4] Columnar and coarse dendritic structures in fusion zones can seriously compromise the mechanical properties of welds.[4–6] Therefore, it would be desirable to replace columnar grains with fine equiaxed ones to improve the weldments' mechanical properties.

It is well accepted that solidification morphology in any given alloy depends on the ratio of G/R, where G is the thermal gradient and R the solidification velocity.[3–5] In fact, inoculants and supercooling play essential and complementary roles in determining the morphology of microstructure in castings and welds from the perspective of solidification mechanism. Potent inoculants and large degrees of supercooling promote heterogeneous nucleation and the refinement of microstructure in alloys during solidification.[1–13]

Inoculants, *i.e.*, nucleating agents, have been widely used to refine grains of castings and welds.[8–15] The choice of effective nucleating agents predominantly depends on the alloy chemistry, and the resultant grain size varies depending on the type and amount of added inoculants.[4,16–19] Both size and type of inoculants have a significant effect on heterogeneous nucleation rate and the resultant grain size of castings and welds.[16–19]

Lu *et al.*[20,21] observed that carbon inoculation significantly refined the microstructure of Mg–Al alloy castings. The most commonly accepted theory of carbon inoculation is that carbon reacts with Al in the melt creating aluminum carbide (Al_4C_3) particles and α-Mg nucleates at the surface of the Al_4C_3 particles, which promote grain refinement in the Mg–Al alloy system.[20,21] Furthermore, Kim *et al.*[22] proposed a theory of duplex nucleation, according to which, a polygonal Al_8Mn_5 first nucleates on the surface of Al_4C_3 and then α-Mg nucleates on the surface of Al_8Mn_5 in Mn-containing Mg–Al alloy systems. Nimityongskul *et al.*[23] provided direct experimental evidence of this duplex nucleation model in AM60B castings.

The effect of a titanium compound addition in the form of Al-3Ti-3B[19,24] and Al-10Ti[15] as a solute on the microstructure of aluminum[16,19,24,25] and Mg alloy castings[15] has been studied. Growth restriction factor (GRF) is commonly used to estimate the efficiency of the added elemental solute to refine microstructure.[8,10,15,19] It was demonstrated that titanium (Ti) is the most effective solute element at reducing the grain size of

L. XIAO and L. LIU, PhD Candidates, S. ESMAEILI, Assistant Professor, and Y. ZHOU, Professor, are with the Department of Mechanical & Mechatronics Engineering, University of Waterloo, Waterloo, ON N2L 3G1, Canada. Contact e-mail: nzhou@mecheng1.uwaterloo.ca

Manuscript submitted November 23, 2010.
Article published online September 15, 2011

aluminium alloys in terms of the GRF.[19] Wang *et al.*[15] studied the effects of Ti addition as a solute in the form of the Al-10Ti in a low-frequency electromagnetic casting process on the grain refinement of AZ31 Mg alloy. The grain refinement was related to the potency of the nucleant and the degree and rate of development of constitutional supercooling generated by the Ti solute elemental rejection during growth of previously nucleated grains.[15]

To the authors' knowledge, little information is available on the effect of pure Ti particles as an inoculant on the microstructure of Mg alloy welds. In our previous articles,[1,2] the preexistence of the coarse Al_8Mn_5 intermetallic phases as an inoculant was observed to promote the columnar-equiaxed transition and microstructure refinement of AZ31 Mg alloy welds. Consequently, the mechanical properties of welds were enhanced. The objective of this work is to study the effect of extraneous Ti addition as an inoculant on the microstructure refinement and mechanical property improvement of AZ31 alloy welds that did not contain coarse Al_8Mn_5 second phase particles.[1]

Although the grain refinement by inoculants with varying potency in Mg-Al alloys has been studied by several investigators,[8–16,21–23,26] the mechanism of grain refinement is still unclear. The further objective of this article is to analyze the relationship between the type and size of inoculants and supercooling, and their effect on the heterogeneous nucleation behavior and microstructure refinement in the fusion zone of AZ31 Mg welds.

II. EXPERIMENTAL PROCEDURE

A. *Resistance Spot Welding and Mechanical Property Measurement*

The material selected in this work was commercial-grade hot-rolled sheets of AZ31 magnesium (Mg) alloy in H24 temper supplied by Posco (Pohang, Korea). The analyzed chemical composition of this alloy (wt pct) was Mg, 3.02 Al, 0.80 Zn, 0.3 Mn, and 0.01 Si.

Rectangular welding specimens of 100 mm × 25 mm × 1.5 mm were prepared parallel to the rolling direction of the sheets. The configuration and dimensions of the welds were described in the previous article.[2] The surfaces of the plates were cleaned chemically using a solution of 2.5 g chromic oxide and 100 mL distilled water to minimize surface oxide and contamination before welding.

The spot welding was carried on a conventional RSW Medweld 3000S D.C. spot welding machine. Truncated cone electrode caps (FF25) with a spherical radius of 50.8 mm and a face diameter of 16 mm, manufactured from class Cu–Cr–Zr alloy, were used. Titanium powder with a purity of 99.98 pct and a size of less than 20 μm in diameter were doped at the designed fusion zone on the interior surface of sheets before welding. The fusion zone was positioned by a model insulator sheet containing a hole, which has the same diameter with the electrode, at the designed fusion zone. This model sheet was removed to the outside of the welding sample and used to determine the welding zone by fitting the hole of the model insulator sheet on the electrode to keep the fusion zone form in the central area of the powder addition. Ti particles were shaped irregularly and polycrystalline; 8 to 10 mg of Ti powder was added to each nugget. The volume fraction of Ti inoculant in the fusion zone was estimated using a polished planar cross-sectional specimen of a nugget by the manual point count procedure according to standard ASTM E562-05, and was found to be about 0.5 pct. The welding conditions are listed in Table I.

The welding current was varied from 22 kA to 32 kA. Six samples were welded under each welding condition: four for the tensile-shear test, one for the measurement of nugget diameter, and one for the examination of microstructure. The nugget diameters were measured using metallographic specimens.

The mechanical properties of the as-received sheets were measured on an Instron 4206 universal test machine (Norwood, MA) at a constant cross-head speed of 10^{-2} mm/s using tensile specimens of dimensions 100 mm × 25 mm × 1.5 mm. The tensile-shear properties of welds were measured using a conventional tensile testing method. The standard tensile loading procedure applied along the longitudinal axis of welding samples produces tensile-shear stress in the welds. Special care was taken to minimize the effect of misalignment between the axis of the nugget and the bonding axis. Shims were used on both ends of the welded specimens to minimize extraneous bending moments.

B. *Microstructural Examination and Temperature Measurement*

All specimens for metallographic and scanning electron microscopy (SEM) examinations were cut, cold-mounted, ground, mechanically polished, and then chemically polished for 5 seconds in 10 pct nital followed by etching for 5 seconds with a solution of 4.2 g picric acid, 10 mL acetic acid, 70 mL ethanol, and 10 mL water. The microstructures of AZ31 welds without and with the addition of Ti were examined using an optical microscope and a JEOL JSM-6460 scanning electron microscope (JEOL Ltd., Tokyo, Japan) equipped with an Oxford ultra-thin window detector energy-dispersive spectrometer (EDS). An X-ray microanalysis was performed using a Rigaku AFC-8 diffractometer (The Woodlands, TX) with Cu target, 50 kV acceleration voltage, and 40 mA current.

The temperature as a function of time in the central area of fusion zone in AZ31 Mg alloy welded at 26 kA

Table I. Welding Parameters Selected in this Work

Welding Current (kA)	Electrode Force (kN)	Welding Time (cycles)	Squeezing Time (cycles)	Cooling Time (cycles)
22-30	4	8	30	30

held for 8 cycles was measured by means of K-type chromel-alumel thermocouple of 10 μm in diameter, which was protected by ceramic tube and preplaced in the central area of fusion zone by drilling a fine tunnel on the side of sample. The data acquisition was carried out with a computer, which was interfaced with Lab-VIEW 8 software (National Instruments Corporation, Austin, TX). The detailed measurement process will be described elsewhere.

C. *Transmission Electron Microscopy (TEM) Foil Preparation and Analysis*

The as-received AZ31 Mg alloy and the added second-phase particles were analyzed using TEM. To analyze the orientation relationship between the added Ti particles and the Mg matrix, TEM foils containing second-phase particles were prepared using the focused ion beam (FIB) (Zeiss NVision 40 [Carl Zeiss, Chicago, IL] FIB/field emission-SEM) technique according to an *in situ* lift-out method.[27] A carbon coating was deposited prior to FIB milling to protect the particle surfaces and the area of interest upon exposure to the Ga+ beam. Once the TEM foil was attached to the grid, final thinning was performed on the lamella, initially at an acceleration voltage of 30 kV, and finally at a low voltage of 1 kV because the milling of the Mg matrix is much faster than that of Ti particles. Details of this procedure can be found in Reference 27. The second-phase particles and their interfaces were observed with a JEOL JEM-2010F field emission transmission electron microscope operated at 200 kV.

III. RESULTS

A. *As-Received Materials*

A typical three-dimensional optical microstructure of AZ31 Mg alloy in the as-received condition is shown in Figure 1. This alloy is composed of equiaxed grains with an average grain size of 7.5 μm. On a close examination, the grain size was not homogeneous. Some grains were elongated along the rolling direction and distributed in the form of strips inside the sheets. TEM examination showed that the microstructure in the as-received AZ31 Mg alloy consisted of an α-Mg matrix, submicron-sized body-centered cubic β-phase $Mg_{17}Al_{12}$ precipitates, and submicron-sized Al_8Mn_5 paticles. The detailed analysis was described in a previous articles.[1]

The tensile stress–strain data of as-received AZ31 Mg alloy sheets were measured and listed in Table II.

The yield strength ($\sigma_{0.2}$) of this alloy is 256 MPa, the UTS is 292 MPa, and the elongation is 20 pct, which are slightly higher than those for this alloy with a standard H24 temper designation.

B. *Weld Microstructures*

1. *Optical microstructure*

A comparison of optical microstructures on the cross-sections of AZ31 alloy specimens welded without and with an addition of Ti powders is shown in Figures 2(a) and (b) and Figures 3(a) and (b). In both conditions, the microstructure could be distinguished with columnar dendritic zone (CDZ) and equiaxed dendritic zone (EDZ) in the fusion zone. The grain structures close to the fusion boundary of the welds were dominated by epitaxial growth. The structure in the weld without Ti addition primarily consisted of well-developed columnar grains, perpendicular to the fusion boundary in a zone with a width of 580 μm. This region is identified as CDZ in Figures 2(a) and 3(a). In contrast, the CDZ was suppressed significantly to within an area of 320 μm in width in the welds with the addition of Ti powders, as shown in Figure 2(b). A subsequent examination showed that a fine-grained and more randomly oriented dendritic structure with short primary arms replaced the well-developed primary arms in the vicinity of the fusion boundaries of the welds with the addition of Ti powders, as indicated by arrows in Figures 2(b) and 3(b). No obvious long columnar grains were observed in the AZ 31 specimens welded with the addition of Ti.

Toward the central area, the coarse flower-like equiaxed dendrites, which are defined as the EDZ, were formed in the Mg alloy welds both with and without the addition of Ti, as shown in Figures 2(a) and (b), and Figure 4(a) and (b). Furthermore, an analysis showed

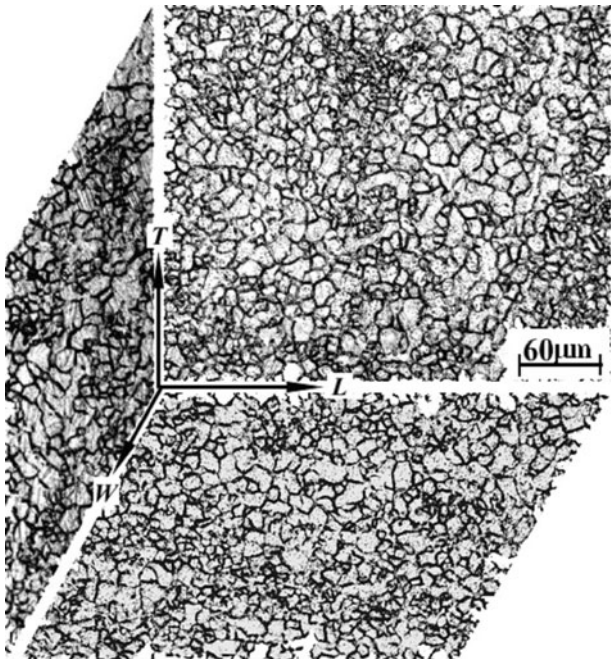

Fig. 1—Optical microstructure of as-received AZ31 alloys in the three cross sections. *L*, The longitudinal axis along the plate rolling direction; *W*, The width axis in the width direction; and *T*, The transverse axis perpendicular to the direction of width.

Table II. Tension Test Results of AZ31Mg Alloy in As-Received Condition

Yield Sress, $\sigma_{0.2}$ (MPa)	Ultimate Tensile Strength (UTS) (MPa)	Elongation, δ (pct)
256	292	20

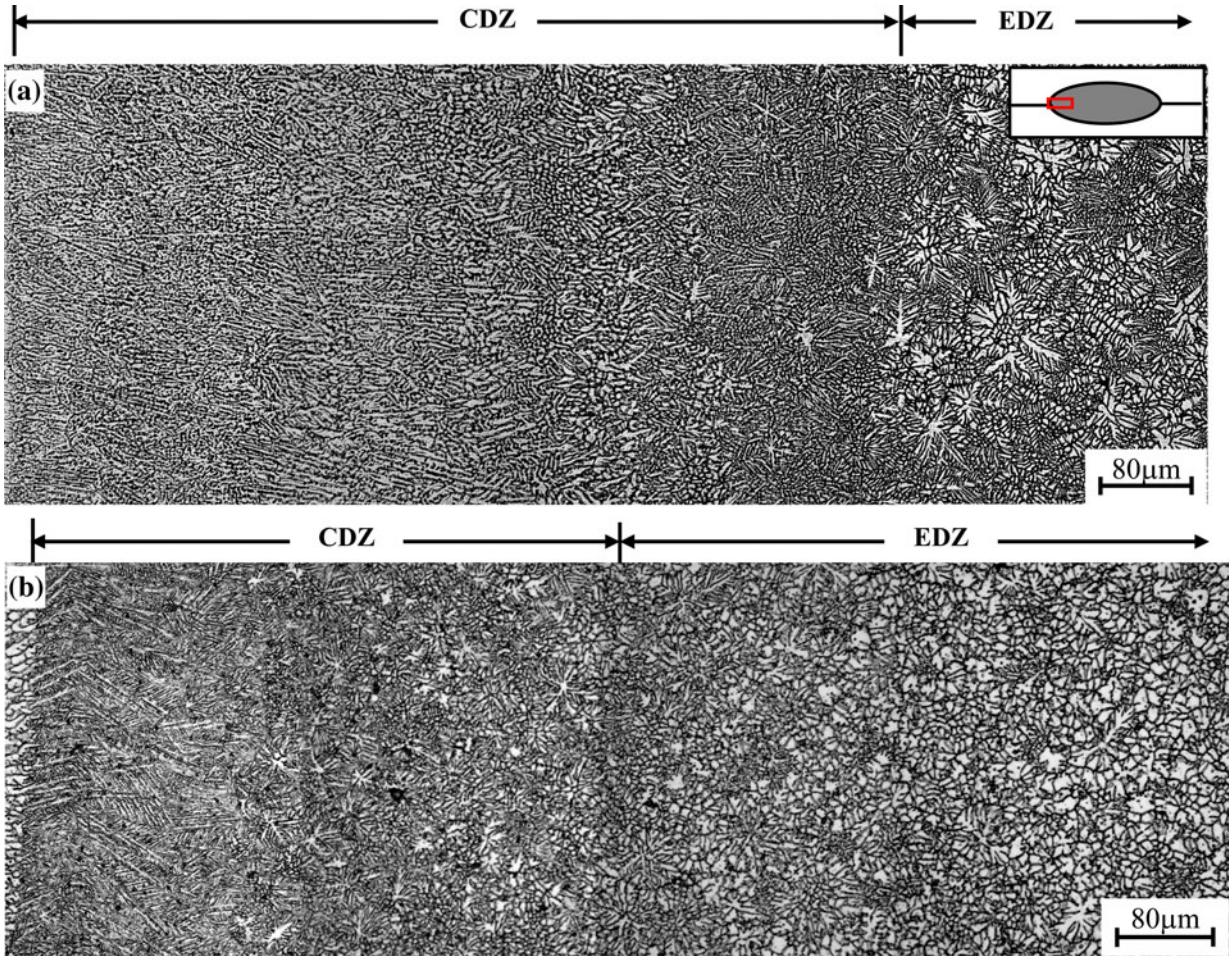

Fig. 2—A comparison of fusion zone microstructure in the AZ31 alloy welded (*a*) without and (*b*) with an addition of Ti.

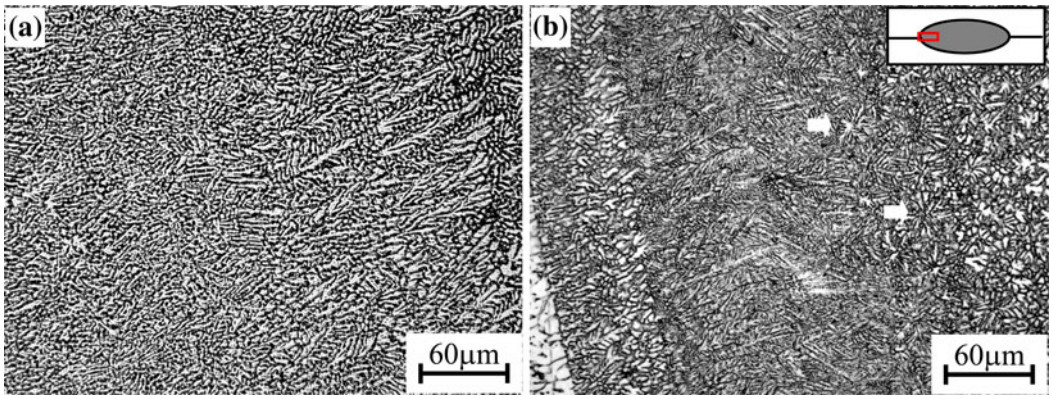

Fig. 3—Effect of Ti addition on the microstructure in the vicinity of the fusion boundary of AZ31 alloy welds: (*a*) without Ti addition and (*b*) with an addition of Ti.

that grain refinement was achieved in the central areas of AZ31 welds with the addition of Ti (Figures 2(b) and 4(b)). The average diameter of the flower-like grains in the welds without the addition of Ti was approximately 65 μm (Figure 4(a)), whereas it was only approximately 20 μm with the addition of Ti (Figure 4(b)). The average primary dendrite arm spacings were measured to be approximately 40 $\pm$ 10 μm in welds without the addition of Ti but only 10 $\pm$ 3 μm when Ti was added.

2. *Ti particles in fusion zones of welds*

SEM examinations showed that Ti particles were successfully introduced into the fusion zones of these welds. Some second-phase particles were observed at the origin of equiaxed dendrites, as indicated by an arrow in Figure 5. The other tiny particles were eutectic $Mg_{17}(Al, Zn)_{12}$ precipitates in the AZ31 Mg alloy.[1] The EDS analysis showed that the large particles were Ti. An analysis of these second-phase particles using EDS line

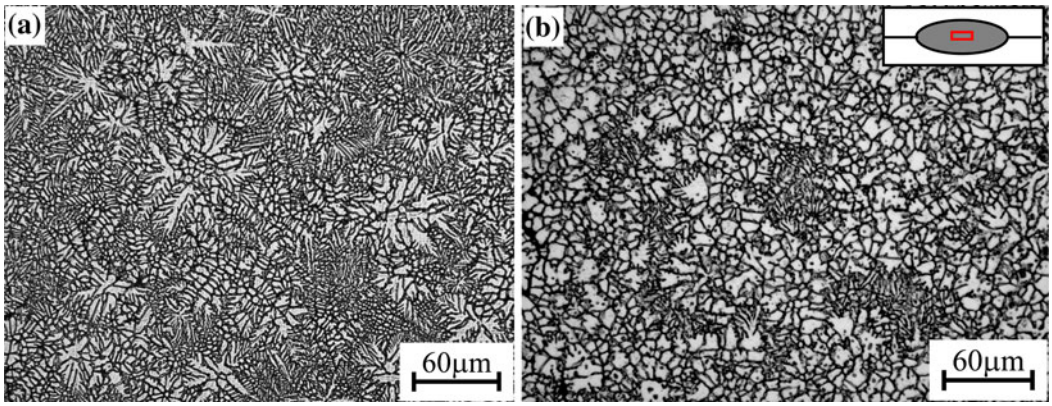

Fig. 4—Effect of Ti addition on the microstructure in the center of AZ31 alloy welds: (*a*) without Ti addition and (*b*) with an addition of Ti.

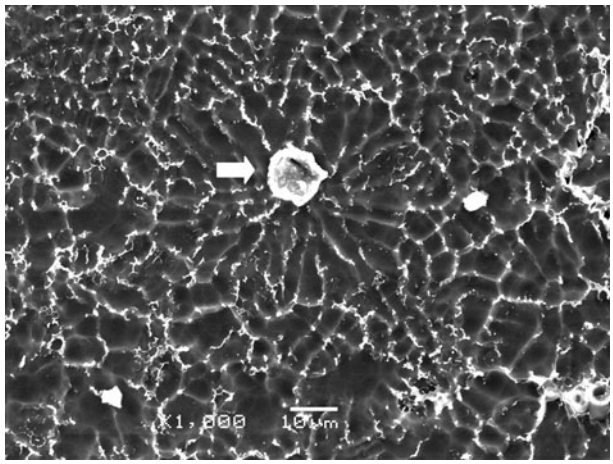

Fig. 5—Equiaxed dendritic grain nucleating on Ti particles in AZ31 welds: (*a*) SEM image and (*b*) EDS.

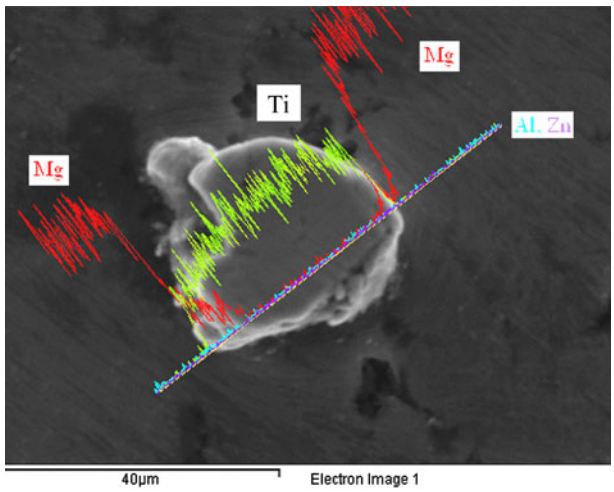

Fig. 6—Line-scan profile of chemical element distribution along the cross section of Ti particles in AZ31 welds.

scanning also demonstrated that these particles were essentially pure Ti particles, as shown in Figure 6. The change of elemental concentration across the interface between particle and matrix was extremely abrupt. This

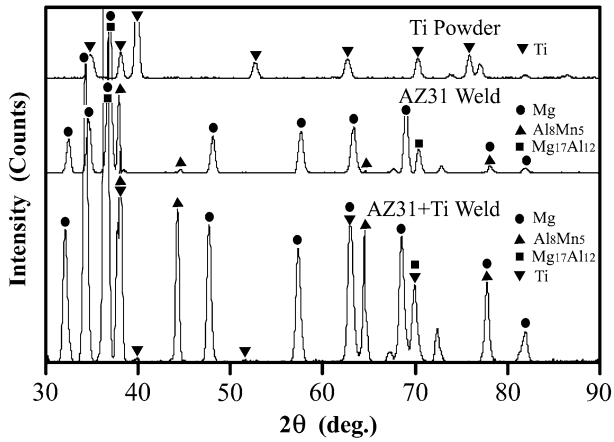

Fig. 7—A comparison of XRD curves of AZ31 alloy welds without and with adding Ti.

implies that chemical reaction between the added Ti particles and alloying elements in the matrix was insignificant.

Figure 7 displays the X-ray diffraction (XRD) results of AZ31 welds without and with addition of Ti powders. For a comparison, the XRD curve of Ti powders was included as well. Some Ti peaks were observed in the welds with added Ti powder, as indicated by down triangles in Figure 7. No XRD peaks of Ti compounds were observed. These results implied that Ti particles were relatively stable in the fusion zone and did not react rapidly with the other alloying elements in the AZ31 Mg alloy during resistance spot welding.

The temperature as a function of time in the central area of fusion zones in Mg alloy welded at 26 kA held for eight cycles is shown in Figure 8. The results revealed that the peak temperature which the fusion zone could reach was approximately 1473 K (1200 °C). The solidification temperature is 873 K (600 °C) during cooling in the current welding condition, as indicated by an arrow in Figure 8. Therefore, spontaneous melting of the added second-phase Ti particles would be unlikely during resistance spot welding because Ti has a melting temperature of 1941 K (1668 °C), which is much higher than what the welding zone could reach. Even though Ti-Mg and Al-Ti system peritectic reactions have low

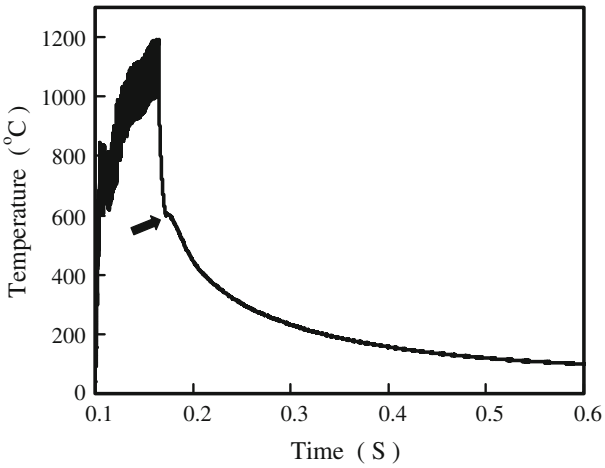

Fig. 8—Typical temperature history curve as a function of time during welding of AZ31 alloy at 26kA in the central area of fusion zone.

temperatures of 924 K (651 °C) and 938 K (665 °C), respectively,[28] the fraction of Ti that could dissolve into the molten pool to beome solute is limited according to Ti-Mg and Al-Ti phase diagrams.[28] As a result, Ti particles could exist in the molten pool in the as-received condition without significantly dissolving or reacting with the other elements during welding.

3. *TEM Analysis*

The microstructure of the added Ti particles and their interfacial characterization with the Mg matrix were analyzed with TEM. Figures 9(a) and (b) demonstrate two typical added Ti particles. The shape of the Ti particles was shown to be polyhedral (Figure 9(a)). Multigrain boundaries were clearly observed inside the added Ti particles, as indicated by arrows in Figures 9(a) and (b). A high density of dislocations were present inside the Ti particles (Figure 9(b)). The interfacial characterization between the Ti inoculant and Mg matrix was examined carefully along different Ti grains, as shown in Figure 10. The orientation relationship between the added Ti particles and Mg matrix in these grains were identified by combining information from several pairs of TEM bright-field images with the associated selected area electron diffraction patterns (SADPs) in Figure 10. In this observed area of a TEM foil, the Ti particle was polycrystalline; in contrast, the Mg matrix was single crystal. Therefore, the foil was tilted until the incident beam was parallel to the $[01\bar{1}0]$ zone axis of the Mg matrix, as shown in Figure 10. The interfacial microstructure and orientation relation between the Mg matrix and the different Ti grains along the Mg/Ti interface were determined sequentially by a series of SADPs. The SADPs of Mg matrix, Ti particle, and the combination of Mg matrix and Ti particle were analyzed at different sites, as indicated by 1 through 8 in Figure 10(a). The SADP analysis results showed that a good orientation relation was only observed in site 3 indicated by an arrow in Figure 10(a). These results are shown in Figures 10(b) through (e). Figure 10(c) showed that the grain of Ti particle in site 3

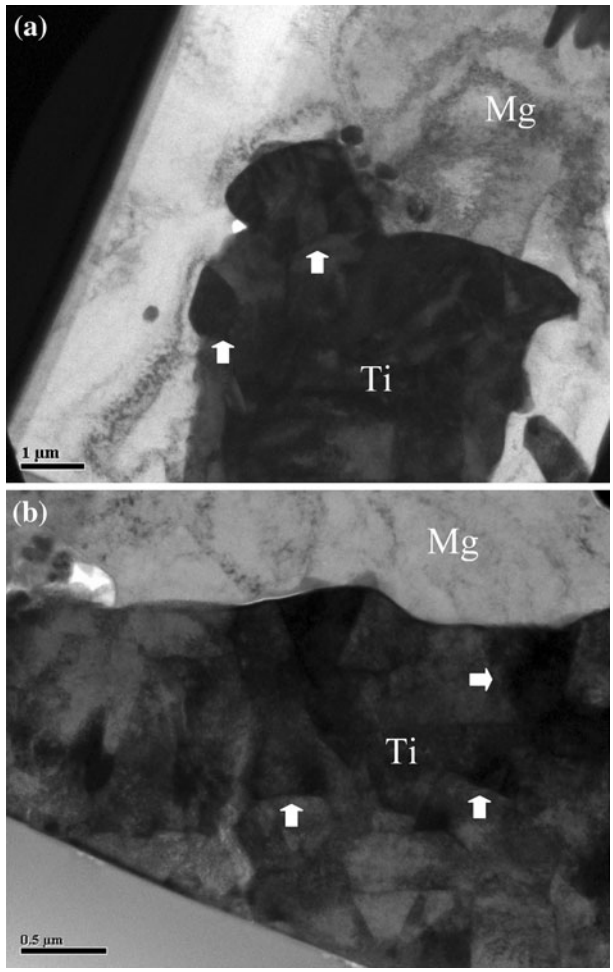

Fig. 9—The added Ti particles inside Mg matrix in the welds: (*a*) polygonal Ti particle and (*b*) grain boundaries inside Ti particle.

was exactly located on $[1\bar{2}1\bar{3}]$ zone axis, when the Mg matrix was parallel to $[01\bar{1}0]$ zone axis. This result implies that the orientation relationship between the added Ti and the Mg matrix on the Ti/Mg interface is $[01\bar{1}0]_{Mg}//[1\bar{2}1\bar{3}]_{Ti}$. Furthermore, the diffraction spot of (0002) of Mg is superposed with that of $(10\bar{1}0)$ of Ti, as shown in Figures 10(d) and (e). This indicates that the crystallographic plane relationship between the added Ti and Mg matrix in this site was determined to be: $(0002)_{Mg}//(10\bar{1}0)_{Ti}$.

The distribution of elements across the interface between the added Ti particle and Mg matrix was analyzed with scanning transmission electron microscopy (STEM)-EDS line scanning, as shown in Figure 11. The results demonstrate that slight interdiffusion of elements was limited within a layer of 30 nm. Chemical reaction between the added Ti particles and alloying elements in matrix essentially did not happen because the element distribution sharply changed across the interface between the added Ti particle and Mg matrix.

C. *Tensile-Shear Properties of Welds*

The tensile-shear testing of resistance spot welds was performed to examine the effect of Ti addition on the

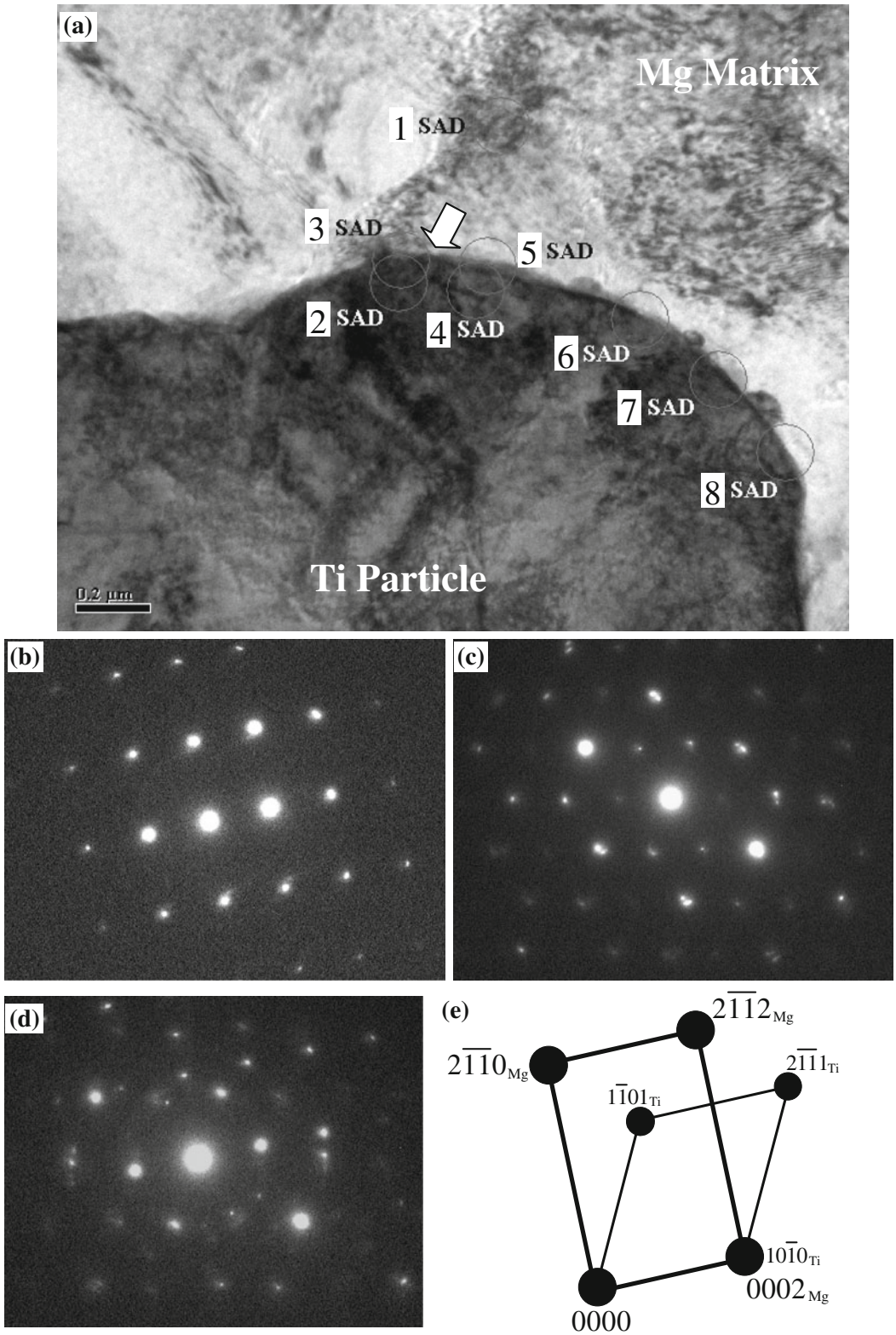

Fig. 10—The interface between the added Ti particle and Mg matrix. (*a*) TEM image; (*b*) SADP of Mg matrix in point 1, incident beam || $[01\bar{1}0]_{Mg}$; (*c*) the corresponding SADP of the added Ti particles, incident beam || $[1\bar{2}\bar{1}3]_{Ti}$ in point 2; (*d*) SADP of the added Ti and Mg matrix in point 3, *i.e.*, the interface between Ti and Mg; and (*e*) its schematic representation in $[01\bar{1}0]_{Mg}$ zone axis in point 3.

mechanical property aspects of weldability of this Mg alloy. Typical load *vs* displacement curves of AZ31 welds are illustrated in Figure 12. The tension-shear mechanical test results presented, each of which are an average of the data of four replicate samples, are summarized in Table III.

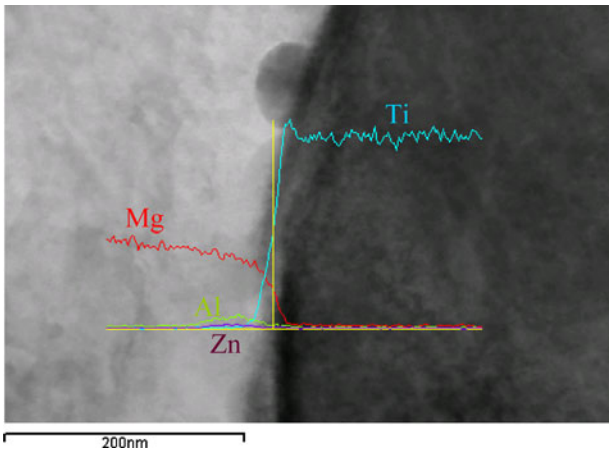

Fig. 11—Line-scan profile of chemical element distribution by STEM-EDS across the interface between the added Ti particles and Mg matrix.

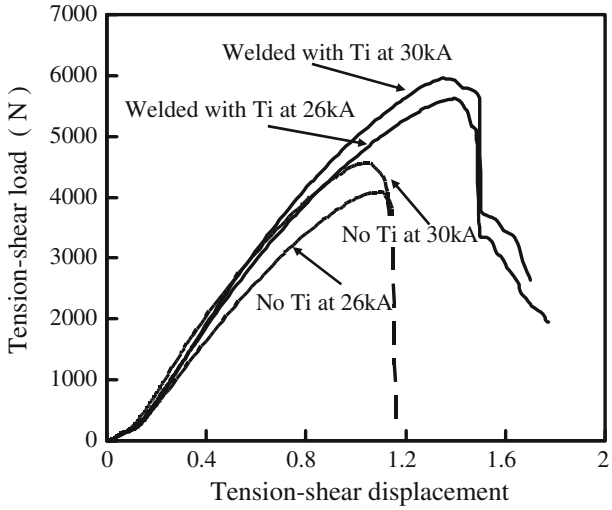

Fig. 12—Effect of Ti addition on tension-shear strength of AZ31 welds.

The ultimate tension-shear load of the alloy welded at 26 kA with an addition of Ti increased by 38 pct from 4076 N to 5619 N in comparison with the welds made without adding Ti. Meanwhile, the displacement rose by 28 pct from 1.09 to 1.40. Thus, both strength and ductility of AZ31 Mg alloy welds were increased by more than 25 pct at a welding current of 26 kA. When the welding current increased to 30 kA, the ultimate tension-shear load of welds with adding Ti increased by 16 pct from 4796 N to 5562 N, and the displacement increased by 17 pct from 1.12 to 1.31.

The added Ti powder could increase the contact resistance between the AZ31 Mg alloy sheets and promote the nugget to grow larger under the same welding current. Our previous experimental results showed that the nugget size of these resistance spot welds almost remained a constant in AZ 31 SB alloy when the welding current was larger than 26 kA.[2] Therefore, the tensile-shear properties of samples welded at high welding currents of 26 kA and 30 kA, resulting in a much similar nugget geometry for resistance spot welds with and without adding Ti inoculants, were selected for comparison. Furthermore, the ultimate tension-shear load was divided by the nugget size to eliminate the possible effect of nugget size. It was confirmed in Table III that the ultimate tension-shear strength of the Mg alloy welds with adding Ti increased by 12 pct and 7 pct compared with those of the welds without adding Ti at 26 kA and 30 kA, respectively. However, the effect of the heat-affected zone (HAZ) on tensile-shear properties of welds is significant when the nugget pullout failure occurs. Subsequent work is needed on the HAZ of AZ31 Mg alloy resistance spot welds, which is beyond the scope of this article.

Table III. Effect of Ti Addition on Tensile-Shear Load and Displacement of AZ31 Welds

Welding Current (kA)	Welding Mode	Ultimate Load (N)	Ultimate Strength* (MPa)	Displacement (mm)
26	no Ti	4076	75	1.1
	added Ti	5619	84	1.4
30	no Ti	4796	76	1.1
	added Ti	5562	81	1.3

*Ultimate strength is the ultimate tension-shear load divided by the area of nugget.

IV. DISCUSSION

A. *Grain Refinement After Ti Addition in AZ31 Welds*

Grain refinement was achieved in AZ31 Mg alloy welds by adding Ti powders into the fusion zones during resistance spot welding. The fine equiaxed dendritic structure formed in the AZ31 welds with an addition of Ti could be ascribed to the heterogeneous nucleation of α-Mg on parts of the surface of the Ti particles, because these particles were observed at the origin of equiaxed dendrites of the matrix as an inoculant by scanning electron microscopy (Figure 5(a)). Moreover, an EDS analysis revealed that the distribution of elements across the interface between Ti particle and Mg matrix showed no transition region of element distribution suggestive of rapid intermetallic formation (Figures 6 and 11). In addition, the experimental measurement of temperature also showed that the peak temperature which the fusion zone could reach was below the melting point of Ti metal (Figure 8). Therefore, these added Ti particles could be expected to survive and become inoculants to promote the nucleation of new grains in the fusion zone of Mg alloy welds, and this heterogeneous nucleation evidently promotes the transition of microstructure from columnar structure to equiaxed structure in AZ31 welds (Figures 2 and 3). The columnar-equiaxed transition mechanism resulting from micron-size second-phase particles has been discussed in Reference 1.

Supercooling is another essential factor to control heterogeneous nucleation and microstructure refinement of alloys. Besides being an inoculant, the added Ti

particles could slightly dissolve into the molten pool to become solute because of the possible Ti-Mg and Al-Ti peritectic reactions.[28] However, it was reported that when the cooling rate was as low as 1.2 °C/min, the resulting constitutional supercooling produced by solute zirconium in Mg alloy was measured to be less than 2.01 °C.[29] The cooling rate could reach 4×10^5 °C/min during resistance spot welding of AZ31 Mg alloy based on our numerical simulation results. The degree of thermal supercooling increases with the cooling rate according to the Hunt's thermal model.[30] As a result, the supercooling produced by constitutional element segregation is much lower than the possible value of thermal supercooling during resistance spot welding. In other words, even though the added Ti particles could dissolve partially into the melt pool of AZ31 Mg alloy welds, the supercooling degree produced by any Ti solute should be much less than thermal supercooling during resistance spot welding. Therefore, the effect of Ti as a solute is much limited compared with that as the inoculant in this work.

Because the values of both G and R are affected by the geometry of the fusion boundary, both the solidification structure and the morphology are affected by the nature of the fusion boundary.[3–5,31,32] Differences in the peak temperature experienced by the material, the cooling rate, and composition at different locations will lead to the formation of varying microstructures along the weld pool centerline. Subsequent studies on the effect of Ti addition on welding variables, temperature distribution, the fusion boundary, and width and shape of the fusion zones of the weldment are needed.

B. *Crystallographic Analysis of Grain Refinement After Ti Addition*

A TEM examination showed that an orientation-matching relationship was determined between the added Ti particles and Mg matrix in some grains of Ti. Meanwhile, a microstructural examination showed that the added Ti particles were observed frequently at the center of the α-Mg grains. It is, therefore, reasonable to assume that the surfaces of the added Ti particles provided suitable nucleation sites for Mg matrix during the solidification of welds.

Turnbull and Vonnegut[33] proposed that the effectiveness of a substrate in promoting heterogeneous nucleation depended on the crystallographic disregistry between the substrate and the nucleated solid. The degree of mismatch of these parameters, *i.e.*, the disregistry, is expressed as

$$\delta = \Delta a_0 / a_0 \qquad [1]$$

where Δa_0 is the difference between the lattice parameter of the substrate and the nucleated solid for a low-index plane and a_0 is the lattice parameter for the nucleated phase.

Zhang, Kelly, and their colleagues[11,34–36] expanded the lattice matching model to the edge-to-edge matching model, which calculates interatomic spacing misfits along matching directions and mismatches between matching planes. According to the edge-to-edge matching model, the matching directions and matching planes are normally the close or nearly close packed directions and planes.[11,34–36]

As the hexagonal close-packed crystal structure, Mg and Ti have three groups of possible close or nearly close packed directions, *i.e.*, $\langle 11\bar{2}0\rangle$, $\langle 10\bar{1}0\rangle$, and $\langle 11\bar{2}3\rangle$, and four groups of possible close or nearly close packed planes, *i.e.*, base plane, $\{0002\}$, prismatic planes, $\{10\bar{1}0\}$, and pyramidal planes, $\{10\bar{1}1\}$ and $\{10\bar{1}2\}$. The interatomic spacing along these potential matching directions is a for straight atom rows $\langle 11\bar{2}0\rangle$, $0.5a\sqrt{3}$ for zigzag rows $\langle 10\bar{1}0\rangle$ $\langle 10\bar{1}0\rangle$, and $0.5(a^2+c^2)^{0.5}$ for zigzag rows $\langle 11\bar{2}3\rangle$.[36]

The distances between adjacent $\{10\bar{1}0\}$ planes can be either $\sqrt{3}a/6$ or $\sqrt{3}a/3$, respectively. If one considers the two planes spaced $\sqrt{3}a/6$ apart as being one corrugated plane, then the distance between corrugated planes remains a $\sqrt{3}a/2$, whereas the effective atomic density is doubled.[37] Meanwhile, the interplanar spacing is $\frac{ac\sqrt{3}}{\sqrt{4c^2+3a^2}}$ for two corrugated first-order pyramidal planes, $\{10\bar{1}1\}$, and $\frac{ac\sqrt{3}}{2\sqrt{3a^2+c^2}}$ for the corrugated second-order pyramidal planes, $\{10\bar{1}2\}$. The distance between the adjacent $\{0002\}$ base planes is always $c/2$.[37]

The lattice parameters used in the current work are $a = 0.3209$ nm and $c = 0.5211$ nm for Mg and $a = 0.2951$ nm and $c = 0.4684$ nm for Ti.[28] Tables IV and V tabulate the relative interatomic spacing misfits along possible matching directions and interplanar spacing mismatches between possible matching planes between Ti phase and Mg matrix, respectively.

It demonstrates that the minimum interatomic spacing misfit along $\langle 10\bar{1}0\rangle_{Mg}//\langle 11\bar{2}3\rangle_{Ti}$ and $\langle 11\bar{2}3\rangle_{Mg}//\langle 11\bar{2}0\rangle_{Ti}$ between the added Ti particles and Mg matrix is only 4 pct, which is much less than the critical value of 10 pct.[36,38] The selection of 10 pct as the critical interatomic spacing misfit value is based on Van der Merwe's energy calculation[38] to obtain the minimum strain energy along different matching directions. In contrast, the interplanar spacing mismatch is only 2 pct for $\{0002\}_{Mg}//\{10\bar{1}0\}_{Ti}$ and 4 pct for $\{10\bar{1}2\}_{Mg}//\{10\bar{1}0\}_{Ti}$. These interplanar spacing mismatches are much lower than the critical value of 6 pct as well.[36,39,40] The 6 pct is an estimation value through an examination of the reported orientation relationships

Table IV. Interatomic Spacing Misfits along Possible Matching Directions between Ti Phase and Mg Matrix

Matching Directions	$\langle 11\bar{2}0\rangle_{Mg}//\langle 11\bar{2}0\rangle_{Ti}$	$\langle 10\bar{1}0\rangle_{Mg}//\langle 10\bar{1}0\rangle_{Ti}$	$\langle 11\bar{2}3\rangle_{Mg}//\langle 11\bar{2}3\rangle_{Ti}$	$\langle 10\bar{1}0\rangle_{Mg}//\langle 11\bar{2}3\rangle_{Ti}$	$\langle 11\bar{2}3\rangle_{Mg}//\langle 11\bar{2}0\rangle_{Ti}$	$\langle 10\bar{1}0\rangle_{Mg}//\langle 11\bar{2}0\rangle_{Ti}$
Interatomic, Mg	0.3209	0.2779	0.3060	0.2779	0.3060	0.2779
Spacing, nm Ti	0.2951	0.2556	0.2768	0.2768	0.2951	0.2951
Interatomic misfit, pct	8	8	10	4	4	6

between matching planes to form an interplanar matching relationship without large-angle rotation of the matching planes.[39,40] The TEM examination provided evidence for the existence of orientation relationships $(0002)_{Mg}//(10\bar{1}0)_{Ti}$ and $[01\bar{1}0]_{Mg}//[1\bar{2}1\bar{3}]_{Ti}$ between some grains of the added Ti particles and Mg matrix in this work (Figure 10). Therefore, the reason why Ti is an efficient refiner of AZ31 Mg alloy could be explained by this crystallographic matching, which led to a low interfacial energy and promoted the nucleation of Mg matrix on the surface of the Ti inoculants in the period of heterogeneous nucleation. However, it is worth noting that crystallographic matching was observed in partial interfaces between the added Ti particles and Mg matrix. Furthermore, some inoculants, such as Al_8Mn_5 intermetallic compound and pure Mn powder, which have a large theoretical interatomic misfit with Mg matrix according to the edge-to-edge model,[34–36] were observed to refine the microstructure of AZ 31 Mg alloy welds in the fusion zone.[1,2,41] Therefore, a good crystallographic matching between the added inoculants and the refined matrix is a sufficient condition rather than necessary one. Another study is needed to establish the detailed relationship between the crystallographic matching and the potency of inoculants.

C. *Critical Size of Potent Inoculants*

Heterogeneous nucleation would occur ahead of the columnar front once the supercooling suffices to induce nucleation, depending on the inoculant size. The dependence of nucleation efficiency on the size and surface properties of the foreign nucleating particles can be expressed by Fletcher's spherical substrate model,[42,43] which is a basic model for understanding heterogeneous nucleation phenomena.

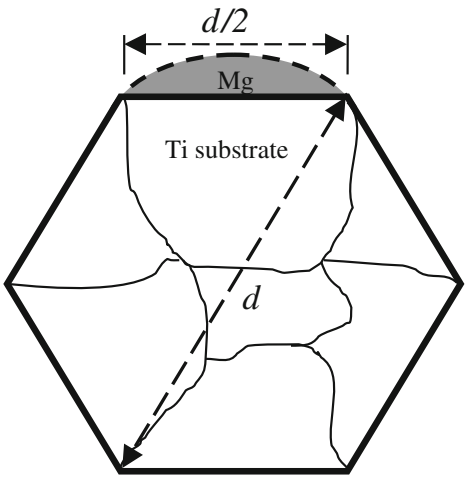

Fig.13—A schematic illustration of a spherical-cap embryo nucleated on one of $\{10\bar{1}0\}$ faces of the added Ti hexagonal platelet particles.

Based on the Fletcher's model, Qian and colleagues[29,42] gave an inverse relationship between the critical nucleation radius r^* and supercooling degree ΔT, in α-Mg:

$$r^* = 0.354/\Delta T \quad [2]$$

Based on TEM results, we simplify the added Ti particles as hexagonal platelets that contain a few $[01\bar{1}0]$ faces where α-Mg nucleation occured. The relationship between the polycrystal Ti particles and Mg embryo can be illustrated schematically in Figure 13. The length of a side of hexagonal platelets is equal to the radius of hexagon, $d/2$.

Based on the Fletcher's classic nucleation theory,[42,43] the substrate radius needs to be at least five times the critical embryo radius to enhance heterogeneous nucleation. Therefore, the size effect of inoculant is most noticeable when $d/2r = 5$, where r is the radius of a spherical embryo. This indicates that the critical size of the added particles as potent inoculants of alloys should be larger than $10r^*$ so that they become the most efficienct refiners.

For the added Ti inoculant with a shape of hexagonal polycrystal platelets, the critical condition for free growth of the crystal through hexagonal platelets should be

$$D = 10r^* \quad [3]$$

Bramfitt[44] measured the supercooling degree of liquid iron added with different inoculants during solidification and suggested the following empirical equation between supercooling and lattice disregistry:

$$\Delta T_c = \delta^2/8 \quad [4]$$

The TEM examination in this work showed that two sets of orientation relationships are present between the added Ti particle and Mg matrix, *i.e.*, $(0002)_{Mg}//(10\bar{1}0)_{Ti}$ and $[01\bar{1}0]_{Mg}//[1\bar{2}1\bar{3}]_{Ti}$. The interplanar and interatomic disregistry between them were calculated to be 2 pct and 4 pct, respectively (Tables IV and V). Therefore, substituting the interplanar disregistry and interatomis misfit with 2 pct and 4 pct, into Eq. [4],

Table V. Interplanar Spacing Mismatches between Possible Matching Planes of Ti Phase and Mg Matrix

Matching Planes	$\{0002\}_{Mg}//\{0002\}_{Ti}$	$\{10\bar{1}0\}_{Mg}//\{10\bar{1}0\}_{Ti}$	$\{10\bar{1}1\}_{Mg}//\{10\bar{1}1\}_{Ti}$	$\{10\bar{1}2\}_{Mg}//\{10\bar{1}2\}_{Ti}$	$\{0002\}_{Mg}//\{10\bar{1}0\}_{Ti}$	$\{10\bar{1}1\}_{Mg}//\{10\bar{1}0\}_{Ti}$	$\{10\bar{1}1\}_{Mg}//\{0002\}_{Ti}$
Interplanar, Mg	0.2605	0.2779	0.2452	0.1901	0.2605	0.2452	0.2452
Spacing, nm Ti	0.2342	0.2556	0.2243	0.1727	0.2556	0.2556	0.2342
Interplanar mismatch, pct	10	8	9	9	2	4	4

supercooling is 0.5 deg for interplanar disregistry and 2 deg for interatomic disregistry.

According to Eq. [2], the critical nucleation radius r^* is calculated to be 0.708 μm and 0.177 μm when the supercooling is 0.5 deg and 2 deg, respectively. Furthermore, based on Eq. [3], the critical size of potent Ti inoculant is estimated to be in the range of 1.8 to 7 μm.

This result demonstrates that the critical size of the added Ti particles should be larger than 1.8 μm to refine the grain size of Mg matrix effectively. Therefore, when Ti particles of ~8 μm in diameter were added into the molten pool, they could become potent inoculants by providing heterogeneous sites for new grain nucleation.

In this work, only a low degree of supercooling is required for the nucleation of Mg matrix on the surface of Ti particles because the added Ti particles have a matching well with the refined Mg matrix. The cooling rate of AZ31 Mg alloy welds during resistance spot welding is high enough to satisfy this requirement of supercooling.

D. *Strengthening Mechanisms of AZ31 Welds with the Addition of Ti*

The results of a tensile-shear measurement revealed that the strength and ductility of AZ31 Mg alloy welds were improved with the addition of Ti particles. This can be attributed to the refinement of grain size and morphology in the fusion zone in these welds.[44] It is well accepted that the finer grain size corresponds to the higher yield strength and ductility.[1,2,45] In contrast, the microstructural characterization of the materials revealed a reasonably uniform distribution of Ti particles with good interfacial integrity between the matrix and the added phases (Figures 5, 6, 9, 10, and 11). The Ti particles are harder than the matrix of Mg. The harder Ti particles in the fusion zones are also expected to provide dispersion strengthening as reinforcement, *i.e.*, Orowan strengthening.[46]

Fine grain formation during solidification promotes the flow of molten metal to feed shrinkage, resulting in smaller and more uniformly dispersed shrinkage or gas porosity. Fine grains also provide a complex network of grain boundaries, reducing the tendency for segregation of alloy elements.[4,47] These factors contribute to the improvement of strength and ductility of welds, as well.

V. SUMMARY AND CONCLUSIONS

1. The fusion zone of AZ31 magnesium alloy resistance spot welds could be divided into CDZ and EDZ. The CDZ produced in the vicinity of the fusion boundaries of the as-received AZ31 Mg alloy welds was suppressed significantly to within a width of 320 μm after the addition of Ti powders. A more randomly oriented dendritic structure with short primary arms replaced the well-developed primary arms in the welds with the addition of Ti powders.
2. The EDZ was formed in the central regions of Mg alloy welds both without and with the addition of Ti. The coarse equiaxed dendrites in the welds without the addition of Ti were refined efficiently by adding titanium powders into the molten pool. The average diameter of the flower-like equiaxed dendrites in the welds with Ti addition was much smaller than that without the addition of Ti. It was approximately 65 μm in AZ31 without the addition of Ti, whereas only approximately 20 μm with the addition of Ti.
3. The ultimate tension-shear load of the AZ31 alloy welded at 26 kA with an addition of Ti increased 38 pct from 4076 N to 5619 N in comparison with the welds without adding Ti. Meanwhile, the displacement increased by 28 pct from 1.09 to 1.40. When the welding current increased to 30 kA, the ultimate tension-shear load increased by 16 pct from 4796 N to 5562 N, and the displacement increased by 17 pct from 1.12 to 1.31.
4. Ti inoculant could provide potent heterogeneous nucleation sites for the Mg matrix because of a good crystallographic matching between some grains of the added Ti particles and Mg matrix. The orientation relationship between those Ti grains and AZ 31 Mg alloy matrix was determined to be $[01\bar{1}0]_{Mg}//[1\bar{2}1\bar{3}]_{Ti}$ and $(0002)_{Mg}//(10\bar{1}0)_{Ti}$.
5. It is suggested that the diameter of the added Ti inoculant should be larger than 1.8 μm to promote efficient nucleation of fine Mg grains. The refined microstructure in the fusion zone could contribute partially to the improvement of tensile-shear properties of AZ 31 resistance spot welds, even though the effect of the HAZ on tensile-shear properties of welds is significant when the nugget pullout failure occurs.

ACKNOWLEDGMENTS

This research is supported financially by the Natural Sciences and Engineering Research Council (NSERC) of Canada in the Framework of Strategic Magnesium Network Program (MagNet) and AUTO21 Network of Centres of Excellence of Canada. L.X. thanks NSERC for a Postgraduate Scholarship. We thank Dr. Julia Huang and Mr. Fred Pearson from Canadian Center for Electron Microscopy, McMaster University for help with preparing TEM films with FIB and TEM observation. Appreciation is also expressed to Dr Xiang Wang, McMaster University, for useful discussions on TEM analysis.

REFERENCES

1. L. Xiao, R. Liu, Y. Zhou, and S. Esmaieli: *Metall. Mater. Trans. A*, 2010, vol. 41A, pp. 1511–22.
2. L. Liu, L. Xiao, J.C. Feng, Y.H. Tian, S.Q. Zhou, and Y. Zhou: *Metall. Mater. Trans. A*, 2010, vol. 41A, pp. 2642–50.
3. S. Kou: *Welding Metallurgy*, 2nd ed., Wiley, Hoboken, NJ, 2003.
4. S.A. David and J.M. Vitek: *Int. Mater. Rev.*, 1989, vol. 34, pp. 213–45.
5. T. DebRoy and S.A. David: *Rev. Mod. Phys.*, 1995, vol. 67, pp. 85–112.

6. J.C. Feng, Y.R. Wang, and Z.D. Zhang: *Sci. Tech. Weld. Join.*, 2006, vol. 11, pp. 154–62.
7. J.C. Villafuerte and H.W. Kerr: *Metall. Trans. A*, 1990, vol. 21A, pp. 979–86.
8. D.H. St. John, M. Qian, M.A. Easton, P. Cao, and Z. Hildebrand: *Metall. Mater. Trans. A,* 2005, vol. 36A, pp. 1669–79.
9. N. Nishino, H. Kawahara, Y. Shimizu, and H. Iwahori: *Magnesium Alloys and Their Applications*, K.U. Kainer, ed., Wiley-VCH, New York, NY, 2000, pp. 59–64.
10. Y.C. Lee, A.K. Dahle, and D.H. St. John: *Metall. Mater. Trans. A*, 2000, vol. 31A, pp. 2895–2905.
11. P. Cao, M. Qian, and D.H. St. John: *Scripta Mater.*, 2006, vol. 54, pp. 1853–58.
12. D. Qiu, M.X. Zhang, J.A. Taylor, H.M. Fu, and P.M. Kelly: *Acta Mater.*, 2007, vol. 55, pp. 1863–71.
13. T. Laser, M.R. Nurnberg, A. Janz, C. Hartig, D. Letzig, R. Schmid-Fetzer, and R. Bormann: *Acta Mater.*, 2006, vol. 54, pp. 3033–41.
14. Y. Tamura, N. Kono, T. Motegi, and E. Sato: *J. Jpn. Inst. Light Met.*, 1998, vol. 48, pp. 185–89.
15. Y. Wang, X. Zeng, W. Ding, A.A. Luo, and A.K. Sachdev: *Metall. Mater. Trans. A*, 2007, vol. 38A, pp. 1358–66.
16. G.J. Davis and J.G. Garland: *Int. Metall. Rev.*, 1975, vol. 20, pp. 83–106.
17. M. Johnsson: *Z. Metallkd.*, 1994, vol. 85, pp. 781–85.
18. A.L. Greer, A.M. Bunn, A. Tronche, P.V. Evans, and D.J. Bristow: *Acta Mater.*, 2000, vol. 48, pp. 2823–35.
19. M.A. Easton and D.H. St. John: *Acta Mater.*, 2001, vol. 49, pp. 1867–78.
20. L. Lu, A.K. Dahle, and D.H. St. John: *Scripta Mater.*, 2005, vol. 53, pp. 517–22.
21. L. Lu, A.K. Dahle, and D.H. St. John: *Scripta Mater.*, 2006, vol. 54, pp. 2197–2201.
22. Y.M. Kim, C.D. Yim, and B.S. You: *Scripta Mater.*, 2007, vol. 57, pp. 691–94.
23. S. Nimityongskul, M. Jones, H. Choi, R. Lakes, S. Kou, and X. Li: *Mater. Sci. Eng. A*, 2010, vol. 527, pp. 2104–11.
24. P. Mohanty and J. Gruzleski: *Acta Metall. Mater.*, 1995, vol. 43, pp. 2001–12.
25. G.N. Heintze and R. McPherson: *Weld J.*, 1986, vol. 65, pp. 71s–82s.
26. L.A. Tarshis, J.L. Walker, and J.W. Rutter: *Metall. Trans.*, 1971, vol. 2, pp. 2589–97.
27. T.M. Moore: *Microscopy Today*, 2005, vol. 13 (4), p. 40.
28. T.B. Massalski: *Binary Alloy Phase Diagrams*, 2nd ed., ASM International, Materials Park, OH, 1990.
29. M. Qian and A. Das: *Scripta Mater.*, 2006, vol. 54, pp. 881–86.
30. J.D. Hunt: *Mater. Sci. Eng.*, 1984, vol. 65, pp. 75–83.
31. B. Ribic, T.A. Palmer, and T. DebRoy: *Int. Mater. Rev.*, 2009, vol. 54, pp. 223–44.
32. S. Mishra and T. DebRoy: *Mater. Sci. Tech.,* 2006, vol. 22 (3), pp. 253–78.
33. D. Turnbull and R. Vonnegut: *Ind. Eng. Chem.*, 1952, vol. 44, p. 1292.
34. M.X. Zhang and P.M. Kelly: *Acta Mater.*, 2005, vol. 53, pp. 1085–96.
35. M.X. Zhang, P.M. Kelly, Ma Qian, and J.A. Taylor: *Acta Mater.*, 2005, vol. 53, pp. 3261–70.
36. M.X. Zhang and P.M. Kelly: *Acta Mater.*, 2005, vol. 53, pp. 1073–84.
37. L. Xiao and H. Gu: *Metall. Mater. Trans. A*, 1997, vol. 28A, pp. 1021–33.
38. J.H. van der Merwe: *Phil. Mag. A*, 1982, vol. 45, pp. 127–43, 145–57, & 159–70.
39. T. Fujii, T. Mori, and M. Kato: *Acta Metall. Mater.*, 1992, vol. 40, pp. 3413–20.
40. D. Duly: *Acta Metall. Mater.*, 1993, vol. 41, pp. 1559–66.
41. L. Xiao, S. Esmaieli, and Y. Zhou: unpublished research, 2010.
42. M. Qian and J. Ma: *J. Chem. Phys.*, 2009, vol. 130, pp. 214709-1–214709-7.
43. N.H. Fletcher: *J. Chem. Phys.*, 1958, vol. 29, pp. 572–76.
44. B.L. Bramfitt: *Metall. Trans.*, 1970, vol. 1, pp. 1987–95.
45. B.Q. Han and D.C. Dunand: *Mater. Sci. Eng. A*, 2000, vol. 277, pp. 297–304.
46. X.L. Zhong, W.L.E. Wong, and M. Gupta: *Acta Mater.*, 2007, vol. 55, pp. 6338–44.
47. D.G. McCartney: *Int. Mater. Rev.*, 1989, vol. 34, pp. 247–60.